Int. J. Electrochem. Sci., 14 **(2019)** 8579 – 8594, doi: 10.20964/2019.09.06

International Journal of
ELECTROCHEMICAL
SCIENCE
www.electrochemsci.org

A Novel Imidazoline Derivative Used as an Effective Corrosion Inhibitor for Carbon Steel in a CO_2/H_2S Environment

Yuan Lu[1], *Wei Wang*[1], *Chen Zhang*[2] *Jingmao Zhao*[1,3,*]

[1]College of Material Science and Engineering, Beijing University of Chemical Technology, Beijing 100029, China
[2]Sinopec Marking South China Company, Guangzhou 510620, China
[3]Beijing Key Laboratory of Electrochemical Process and Technology for Materials, Beijing 100029, China
[*]E-mail:jingmaozhao@126.com

Received: 4 May 2019/ *Accepted:* 16 June 2019 / *Published:* 31 July 2019

Thioureido-oleic acid imidazoline, TAI, is widely used in the oil/gas industry as an effective corrosion inhibitor to protect carbon steel pipelines from CO_2 corrosion. However, the inhibition efficiency is significantly reduced when H_2S gas coexists with CO_2. In this study, the imidazoline was modified by reaction with formaldehyde and propynyl alcohol to develop a modified imidazoline (MTAI). The inhibition performance was evaluated by dynamic weight loss, potentiodynamic polarization, contact angle, and scanning electron microscopy (SEM) measurements as well as quantum chemical calculations. Dynamic corrosion tests and polarization measurements show that the inhibition efficiency of MTAI is significantly better than that of TAI in a CO_2/H_2S environment. The contact angle measurements show that the MTAI inhibitory film is more hydrophobic than the TAI film. The quantum chemical calculations demonstrate that MTAI has two adsorption centres, which make the adsorption more stable and thus the inhibition more efficient.

Keywords: CO_2/H_2S corrosion; imidazoline; corrosion inhibitor; weight loss; polarization curve; contact angle; adsorption; quantum chemical calculation

1. INTRODUCTION

CO_2 corrosion (also called sweet corrosion) and CO_2/H_2S corrosion (sour corrosion) are frequently encountered in the oil/gas industry [1-4]. In a CO_2/H_2S coexistence system, the interaction of gases makes the corrosion more severe and complex. Even trace amounts of H_2S have a significant impact on CO_2 corrosion, increasing the risk of corrosion failure and promoting localized corrosion [5-6].

Many methods can be used to control corrosion [7-9]. Among them, corrosion inhibitors can effectively inhibit corrosion by forming an inhibitive film on the metal surface, which prevents the

corrosive medium from contacting the metal [10-12]. The use of corrosion inhibitors has advantages that include low cost, simple operation, rapid effect, and long-term protection; therefore, it is one of the most promising measures for protecting oil and gas field equipment [13-20].

Imidazolines and their derivatives are widely used as organic corrosion inhibitors in oil and gas fields worldwide to effectively inhibit CO_2 corrosion [21-27]. Among these compounds, thioureido-oleic acid imidazoline (TAI) has been used successfully in Chinese oilfields to control the corrosion of equipment by CO_2-containing water [28]. Long-term field usage results have proven that TAI is a very good anti-CO_2 corrosion inhibitor. However, in recent years, with the deep exploitation of oilfields, the corrosion inhibition capability of TAI is significantly reduced due to the increased content of H_2S. It is important to modify TAI to improve its anti-sour corrosion performance.

J.M. Zhao et al. [29] synthesized six imidazolines with different pendant chains and investigated their inhibition performances by a weight loss method at three flow rates under a high-pressure CO_2 environment. The results showed that the inhibition abilities of imidazoline were affected by both the chemical structure of the compounds and the flow rate of fluid.

L.M. Rodriguez-Valdez et al. [30] compared the inhibition properties of amidoethyl and hydroxyethyl imidazoline inhibitors in CO_2-saturated brine solution. The results showed that amidoethyl imidazoline has the highest efficiency, whereas hydroxyethyl imidazoline has the lowest efficiency.

K.G. Zhang et al. [31] investigated two halogen-substituted imidazolines in 0.5 M HCl solutions by weight loss, potentiodynamic polarization, and electrochemical impedance spectroscopy (EIS). The results showed that trichloromethyl imidazoline possessed the best inhibition property.

Recently, a coconut oil-modified hydroxyethyl imidazoline was synthesized by Rivera-Grauet et al. and used as an effective corrosion inhibitor in a CO_2/H_2S system to protect carbon steel in 3% NaCl solutions [32]. The inhibition efficiency with only 20 ppm of inhibitor reached 97%.

A novel imidazoline compound containing sulfur was synthesized by S.Q. Hu et al. [33], and the corrosion inhibition performance for mild steel corrosion under the coexistence of H_2S and CO_2 was investigated. The results indicated that the inhibitor had excellent corrosion inhibition performance, reaching a high inhibition efficiency of 92.74% when used at a concentration of 4.0×10^{-3} M.

It is well acknowledged that propargyl alcohol (PA) is the most effective inhibitor for inhibiting the corrosion of carbon steel in HCl solutions, especially at high temperatures. In this work, we intended to develop an effective inhibitor in a CO_2/H_2S system using TAI, PA, and formaldehyde. The inhibition performance was evaluated by dynamic weight loss, potentiodynamic polarization, contact angle, and scanning electron microscopy (SEM) as well as quantum chemical calculations.

2. EXPERIMENTAL

2.1 Solutions and materials

The water for testing was obtained from an oil field in China. Its chemical components are shown in Table 1.

Table 1. Chemical components (mg/L) of the oilfield water

HCO_3^-	Cl^-	SO_4^{2-}	Ca^{2+}	Mg^{2+}	Na^++K^+
2114.96	18106	1123	2049	478	19135

In this work, 20# carbon steel with the chemical composition listed in Table 2 was used. The steel was cut into coupons with a size of 50×10×3 mm for testing weight loss and 10 mm×10 mm×3 mm for electrochemical measurements. Before use, the coupons were mechanically abraded with emery papers up to 2000 grits and then sequentially rinsed with ethanol and acetone.

Table 2. Chemical composition (wt.%) of 20# carbon steel

C	Si	Mn	P	S	Cr	Cu	Ni	Fe
0.22	0.26	0.55	0.02	0.02	0.21	0.20	0.28	remainder

2.2. Synthesis of TAI and MTAI

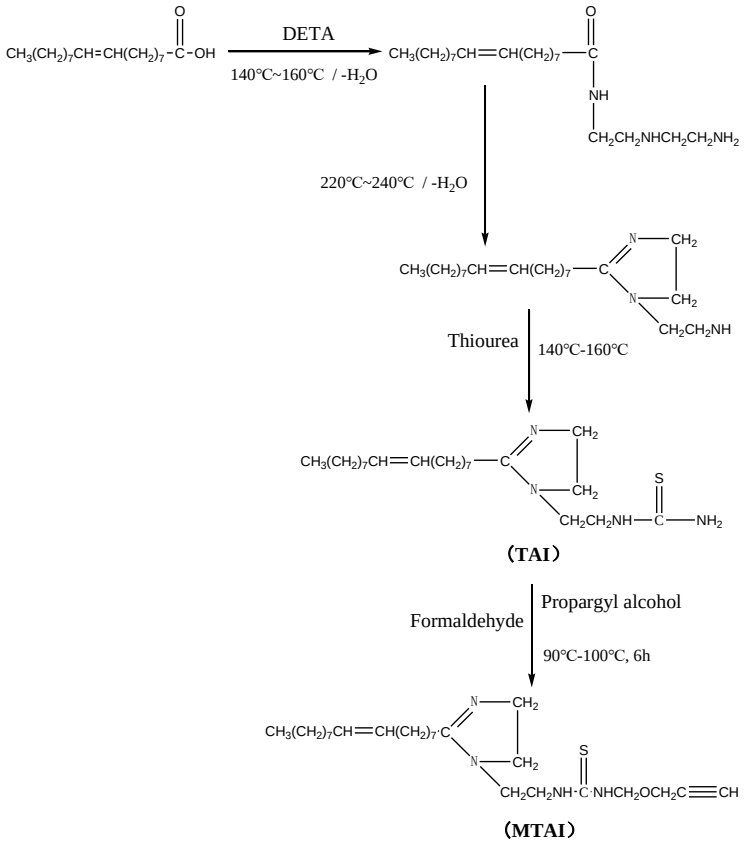

Figure 1. Structural formula of imidazoline derivative and reaction process

Oleic acid and diethylenetriamine were added into a glass flask at a molar ratio of 1:1.2.

Xylene was also added as a water-carrying agent. The reaction temperature was increased to 140-160°C. Four hours later, the temperature was further increased to 220-240°C for another 4 h. Then, the temperature was allowed to decrease to approximately 120°C, and an equimolar amount of thiourea relative to oleic acid was added to the flask. TAI was obtained after reaction at 140-160°C for 10 h.

Finally, PA and formaldehyde were subsequently added to the flask both at an equimolar ratio to oleic acid. The reaction was carried out at 90-100°C for 6 h. The product was named MTAI.

The reaction formula is shown in Figure 1.

The final product was characterized by an AVATA R370 FT-IR system (NICOLET) in a wavenumber range of 400 to 4000 cm^{-1}. MS spectra were obtained on a Waters MALDI Synapt Q-TOF mass spectrometer.

2.3 Dynamic weight loss

The dynamic weight loss test was conducted in an autoclave made of C-276 alloy. The equipment sketch map is shown in Figure 2. After the steel coupons were put into the solution, N_2 was introduced to the solution for 1 h, and the solution was heated to 60°C. Then, a mixture of CO_2/H_2S (H_2S content: 190 ppm, the balance is CO_2) was applied to the autoclave at a pressure of 0.2 MPa with a flow rate of 1.5 m/s. The concentration of the corrosion inhibitor was 50 mg/L.

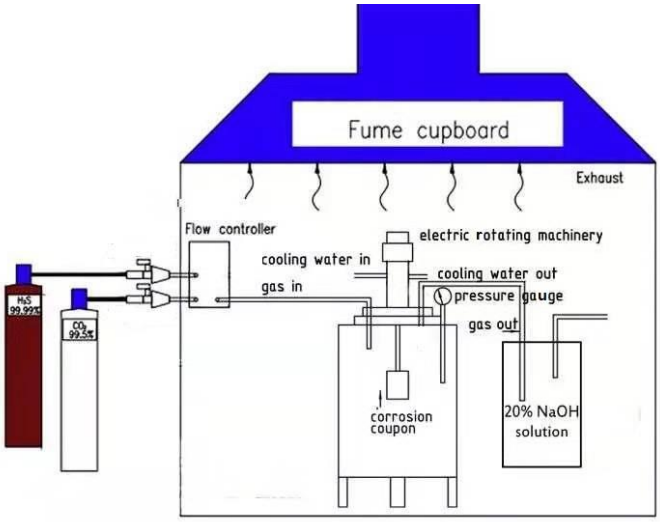

Figure 2. Sketch map of test equipment

After 72 h, the coupons were removed from the solution and immersed in Clarke's solution for 5 min to remove the corrosion products [29]. Next, the coupons were washed with water, degreased in acetone and ethanol, dried by a hot air stream, and then re-weighed.

The mean corrosion rate is obtained by using formula (1).

$$V = \frac{8.76 \times 10^4 \times \Delta W}{s \times t \times \rho} \quad (1)$$

where V is the mean corrosion rate, mm/a; ΔW is the average weight loss of three parallel coupons before and after the test, g; s is the area of the coupon, cm^2; ρ is the density of carbon steel, g/cm^3; and t is the test time, h.

$$\eta = \frac{V_0 - V}{V_0} \times 100\% \qquad (2)$$

where η is the inhibition efficiency; V and V_0 are respectively the mean corrosion rate of steel soaked in the produced water with and without 20 mg/L of inhibitor, mm/a.

2.4 Polarization curve

The potentiodynamic polarization was performed with a CHI604D electrochemical test system. A classical three-electrode cell was used, where a saturated calomel electrode (SCE) was used as the reference electrode, Pt was the auxiliary electrode, and 20# steel was the working electrode. The potential scan range was ±200 mV (relative to the open-circuit potential). The scan rate was 0.167 mV/s. The test temperature was 60°C.

Before measurements, the test solution was de-aerated with N_2 for 1 h, and then the mixture of CO_2/H_2S was bubbled at a flow rate of 50 mL/min through the solution for 1 h. The concentration of the corrosion inhibitor was 50 mg/L.

2.5 Contact angle

After the dynamic weight loss testing, the coupons were removed from the solution, rinsed with deionized water to remove corrosive species, and then dried with hot air. The contact angle measurements were performed with a Dataphysics OCA20 contact angle measuring system.

3. RESULTS AND DISCUSSION

3.1 Structure characterization

Figure 3 shows the infrared spectrum of MTAI. The peaks at 1610.30 cm-1 and 1275.70 cm^{-1} belong to the N=C and C-N tensile vibration peaks, respectively, which are characteristic of imidazoline [34,35]. The peaks at 1457.95 cm^{-1} and 1042.35 cm^{-1} could be assigned to vibrations of C=S [35,36]. The peaks at 3274 cm^{-1}, 2923.60 cm^{-1} and 2849.36 cm^{-1} correspond to the stretching vibration of the N-H bond and the symmetric and asymmetric stretching vibrations of the C-H bond, respectively [29,36]. The absorption peak at 2119.42 cm^{-1} is related to the tensile vibration of triple-bond C≡C [36]. The results indicate the formation of molecules containing acetylenic bonds and imidazoline nitrogen heterocyclic rings.

As shown in Figure 4, the M/Z peak of the product is 463.3, which is in line with the calculated M/Z of $[M+H]^+$($C_{26}H_{47}N_4OS$). Together with the infrared spectrum, the results indicate that the target compound has been successfully synthesized.

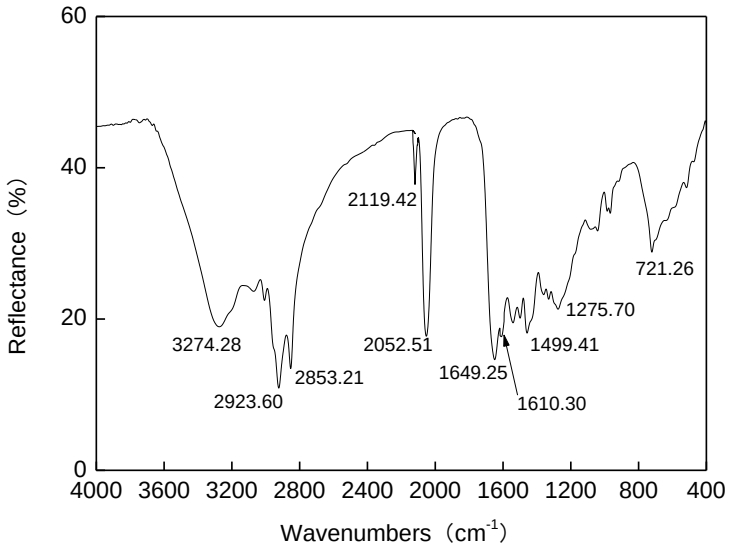

Figure 3. Infrared spectrum of MTAI

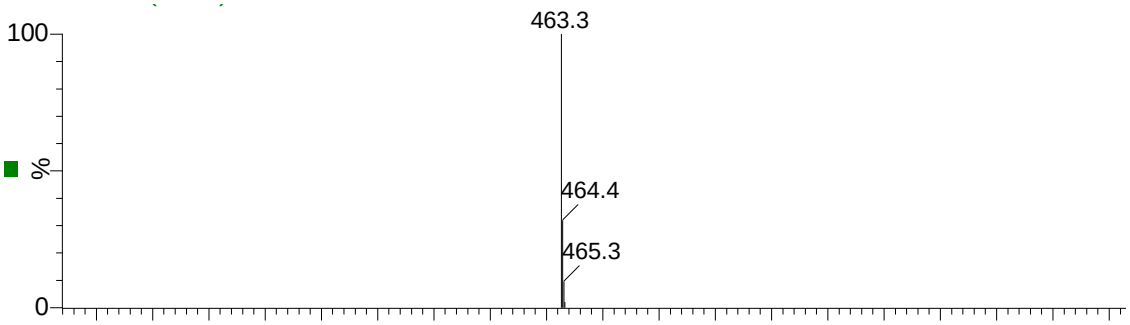

Figure 4. MS-EIS of MTAI

3.2 Dynamic weight loss

The inhibition performances of TAI and MTAI were both evaluated in CO_2 and CO_2/H_2S systems. The results are shown in Table 3. It is found that these two inhibitors can effectively inhibit CO_2 corrosion. For TAI and MTAI, the corrosion rates decrease from 3.580 to 0.119 and 0.096 mm/a, respectively, when the inhibitors are present at a concentration of merely 20 ppm in the solution. MTAI shows better inhibition ability than TAI. Moreover, the inhibition efficiency of TAI is reduced from 96.68% to 79.93% after adding H_2S into the solution at a concentration of 190 ppm. This result is consistent with the actual situation on the site. The inhibition performances of MTAI only change slightly. The inhibition efficiency of MTAI reaches as high as 93.93% in the CO_2/H_2S coexistence system. The other six imidazoline inhibitors (IM, IM-1, IM-2, IM-3, IM-M and IM-OH) synthesized by J.M. Zhao et al. [29] were also tested in CO_2/H_2S systems. The inhibition efficiency of MTAI was better than those compounds. Because MTAI and TAI are the most effective corrosion inhibitors among the eight inhibitors and TAI is the most widely used in offshore oilfields, these two corrosion

inhibitors are mainly studied in subsequent tests.

Table 3. Inhibition efficiencies of two inhibitors in 0.2 MPa CO_2 brine solution (with and without 190 ppm H_2S)

Inhibitor	Concentration of H_2S (ppm)	The mean corrosion rate (mm/a)	η (%)
blank	0	3.580	
TAI		0.119	96.68
MTAI		0.096	97.32
blank	190	2.510	
TAI		0.602	76.01
MTAI		0.152	93.94
IM		0.902	64.06
IM-1		0.881	64.90
IM-2		0.752	70.04
IM-3		0.748	70.20
IM-M		0.835	66.73
IM-OH		0.613	75.58

3.3 Potentiodynamic polarization

The potentiodynamic polarization curves (as shown in Figure 5) were measured in the produced water containing CO_2 and H_2S. The fitted data are listed in Table 4. The polarization results also show that MTAI is clearly better than TAI. The corrosion inhibition efficiency of MTAI reaches 95.37%, which is in good agreement with the results of weight loss. The corrosion potential is significantly shifted to a positive position after addition of the inhibitors, indicating that these inhibitors mainly suppress the anodic dissolution reaction of carbon steel.

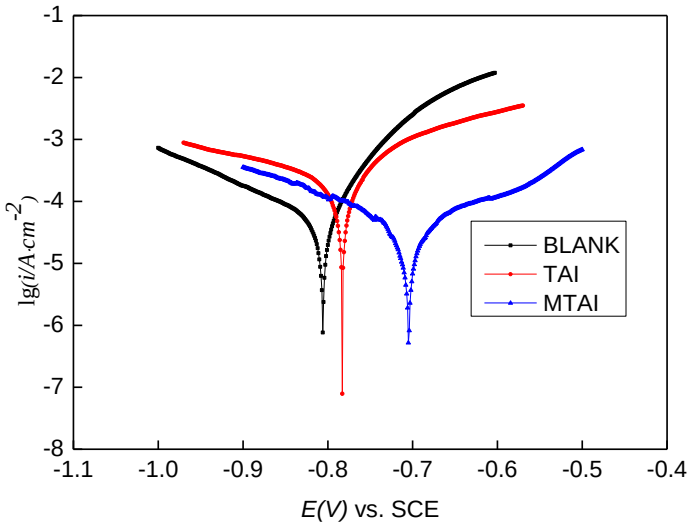

Figure 5. Polarization curves of steel in the CO_2/H_2S produced water with two imidazolines

Table 4. Fitted results of the polarization curves

Solution	ba (mV/s)	bc (mV/s)	Corrosion current density (μA/cm^2)	η (%)
blank	56.58	-198.43	51.44	
TAI	68.44	-123.41	7.08	86.24
MTAI	112.05	-72.34	2.38	95.37

3.4 Contact angle

The contact angles were measured for the steel coupons soaked in the produced water with and without inhibitors. The results are shown in Figure 6.

The contact angle is approximately 60 degrees in the solution with TAI and reaches 69 degrees with MTAI. A larger contact angle indicates a higher degree of hydrophobicity and a denser corrosion inhibitor film [37]. Our previous research showed that the optimal contact angle value is 65-70 degrees [29]. When the contact angle is larger than the optimal value, the dispersion of inhibitors is poor due to the strong hydrophobicity.

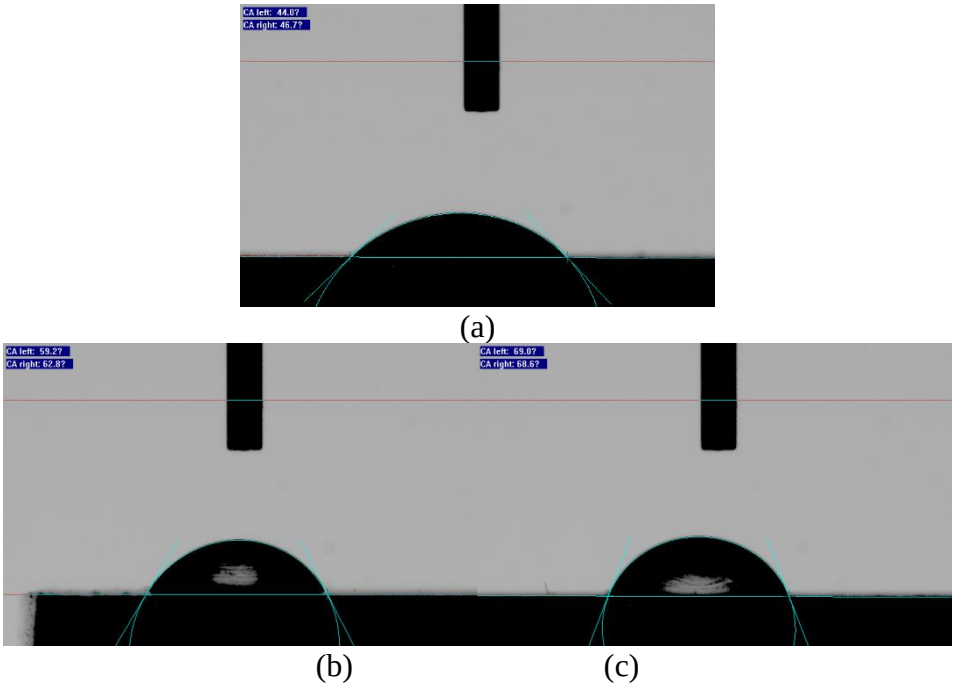

Figure 6. Contact angles on the steel surface soaked in the produced water. a) Without corrosion inhibitor; b) Containing 20 ppm of TAI; c) Containing 20 ppm of MTAI.

3.5 SEM observation

The surface morphologies of carbon steel before and after being immersed in different

solutions for 72 h were observed using SEM. Figure 7(A) shows the surface morphology of the coupon before testing with clearly visible stripes on the surface. Fig. 7(0) shows the surface morphology of the steel in a blank solution. It could be seen that the corrosive medium caused severe damage to the surface of the carbon steel. Figure 7(1) shows the surface morphology of the steel in the solution with 20 ppm TAI. The surface is covered by corrosion products. Figure 7(2) shows the surface morphology of the steel in the solution with 20 ppm MTAI. The stripe on the carbon steel surface is clearly visible, indicating that MTAI has a good inhibitory effect on CO_2/H_2S corrosion.

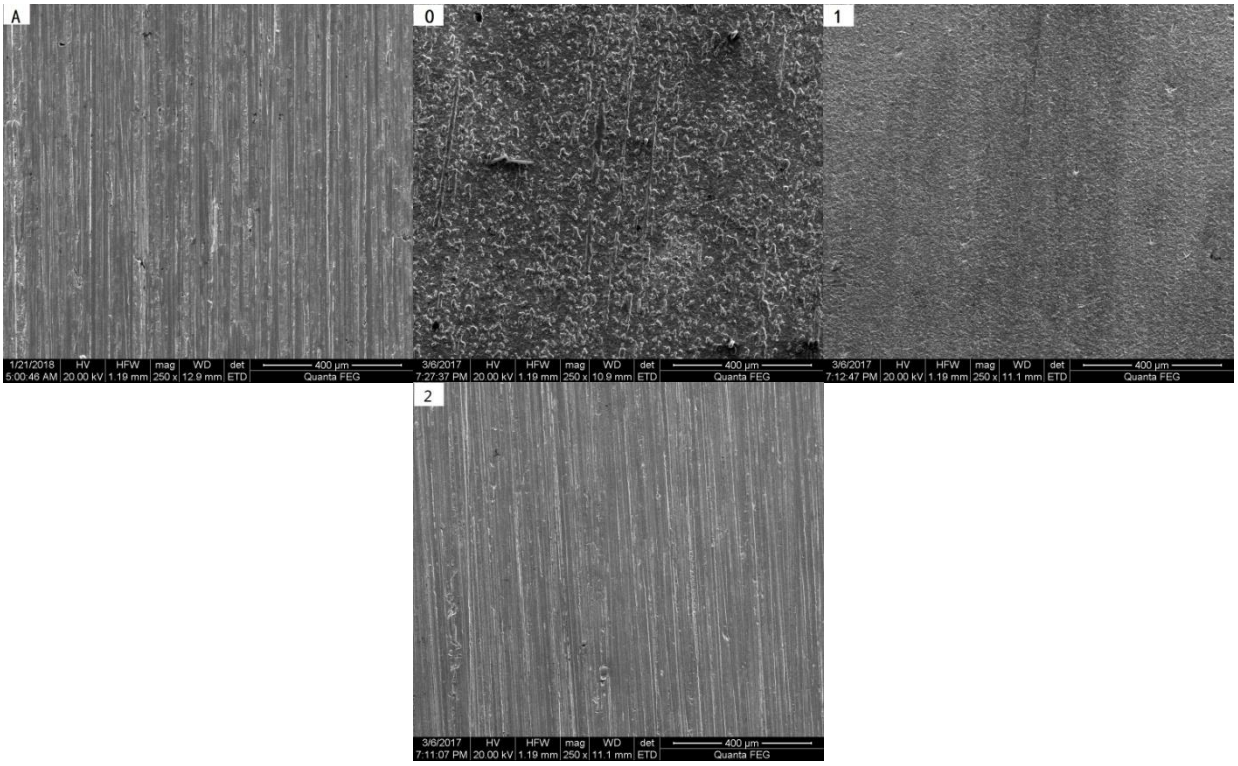

Figure 7. Surface morphologies of steel coupons: (A) before test; (0) the coupons immersed in CO_2/H_2S solutions with no inhibitor (0); (1) with TAI for 72 hours; and (2) with MTAI for 72 hours.

3.6 The adsorption isotherm

To investigate the adsorption behaviour of these two compounds on the steel surface, the inhibition efficiencies of TAI and MTAI at different concentrations were determined by the potentiodynamic polarization method. Figure 8 shows their inhibition efficiencies at different concentrations. It could be seen that the inhibition efficiencies increased rapidly with increasing concentration and remained almost constant when the concentrations exceeded 200 ppm.

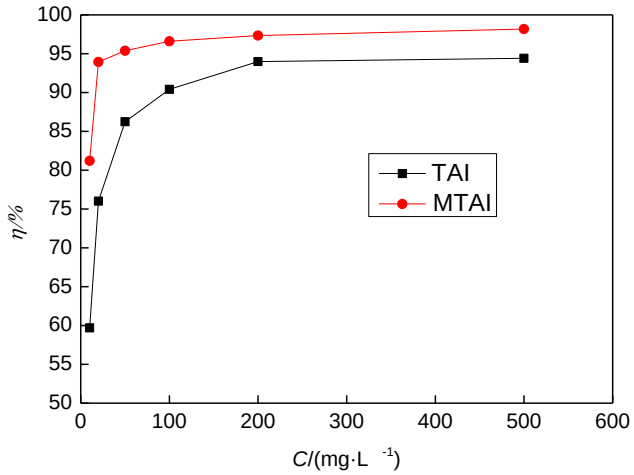

Figure 8. The inhibition efficiencies of TAI and MTAI at different concentrations

The degree of surface coverage (θ) of an inhibitor on the steel surface can be regarded as the inhibition efficiency [38-39]. The experimental data were fitted to a series of adsorption isotherms, and the best fit was obtained with the Langmuir adsorption isotherm (Figure 9), indicating that the adsorption of TAI and MTAI follows Langmuir adsorption [38,39]. The linear regression results are listed in Table 5.

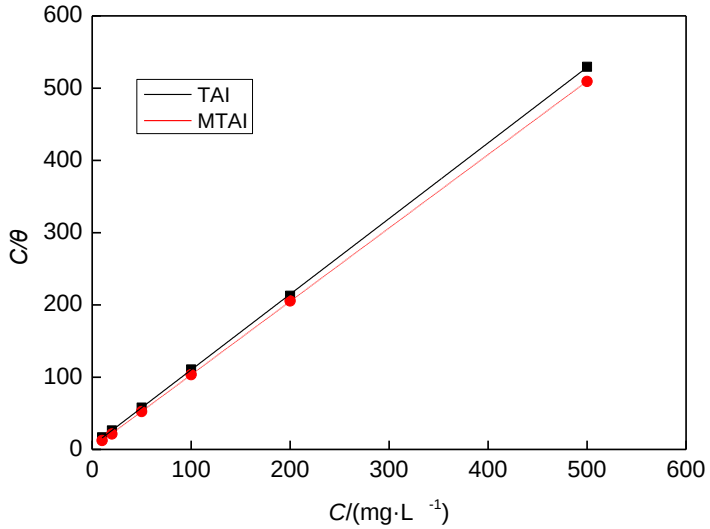

Figure 9. Relationship between C/θ and C of two inhibitors

Table 5. Parameters of the linear regression between C/θ and C

	Adsorptive equilibrium constant, K	Slope	Linear regression coefficient, r
TAI	0.18298	1.04688	0.99996

MTAI	0.56394	1.01556	0.99999

The thermodynamic parameters (ΔG_{ads}) were calculated according to Formula (3)[40-43], with results listed in Table 6. The negative values of ΔG_{ads} indicate that adsorption is a spontaneous process[44-45].

$$K=\frac{1}{10^6}\exp(\frac{\Delta G_{ads}}{RT}) \qquad (3)$$

Table 6. Adsorption free energy (ΔG_{ads}) of TAI and MTAI on the steel surface

Inhibitor	ΔG_{ads}/kJ·mol^{-1}
TAI	-37.08
MTAI	-40.52

When the ΔG_{ads} value is more negative than -40 kJ.mol^{-1}, it indicates the formation of a coordinate type of bond between an inhibitor and metal surface [26]. Therefore, the adsorption of MTAI on the metal surface is of a chemical nature.

3.7 Quantum chemistry calculations

Materials Studio was adopted to obtain information about molecular geometry and electron distribution. The molecules were optimized using the B3LYP functional with the Minimizer in the DMol3 module.

According to frontier orbital theory [46-47], the energy value of the highest occupied molecular orbital (HOMO), E_{HOMO}, indicates the capability of donating electrons to metallic atoms. The energy value of the lowest unoccupied molecular orbital (LUMO), E_{LUMO}, represents the capability of a molecule to accept electrons. The energy gap ΔE, the difference between E_{LUMO} and E_{HOMO}, implies molecular reactivity. A small value of ΔE indicates a strong adsorption and thus a high efficiency of corrosion inhibition. Therefore, E_{LUMO} and E_{HOMO} can be used to determine the reactivity of an inhibitor. The Fukui index can be used to analyse the reactive point, molecular reactivity, and properties of nucleophilic and electrophilic compounds.

The optimized geometries and HOMO and LUMO distributions of the inhibitors are shown in Figures. 10-12. Tables 7-8 lists the orbital energy and the Mulliken charge of non-hydrogen atoms, respectively. From Figures.10-12 and Tables 7-8, the reaction centre of TAI is localized near the sulfur atoms. The inhibition mechanism is mainly the formation of a coordinate bond between the unoccupied d orbital of Fe accepting electrons from the S atom of TAI. Inhibitor molecules are adsorbed on a metal surface to protect metal from corrosion. The ability of the S atom to donate electrons is reduced due to a strong attraction of the C≡C triple bond, resulting in a decrease in the Fukui negative exponent value (f^-) and E_{HOMO}. For MTAI, it has two absorption centres: the sulfur

atom and imidazoline ring. The unoccupied d-orbital of the Fe atoms can accept electrons from the sulfur atom and nitrogen atoms of the imidazoline ring of MTAI to form coordinate bonds. The dual-active adsorption centre makes the ΔE of MTAI significantly lower than that of TAI, indicating that the adsorption film of MTAI is more stable with better inhibition efficiency compared to TAI. The computational results are consistent with results from the dynamic weight loss, polarization curve, and contact angle measurements.

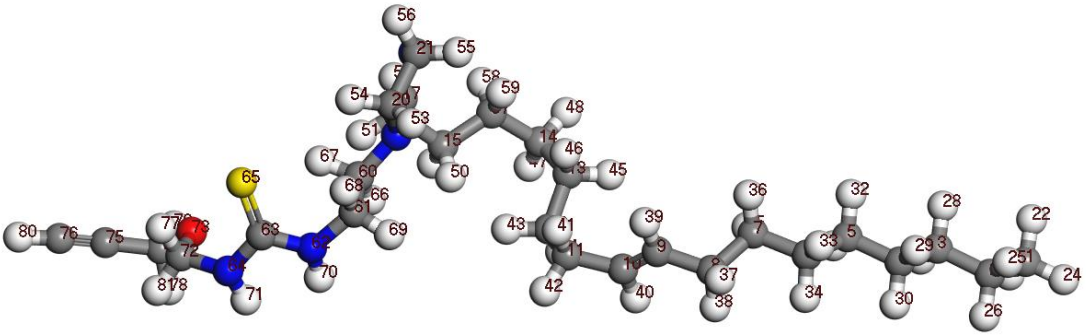

TAI

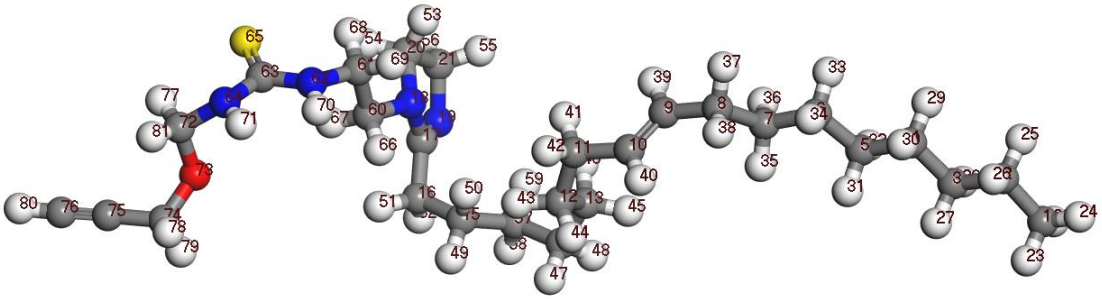

MTAI

Figure 10. Optimized geometries of TAI and MTAI

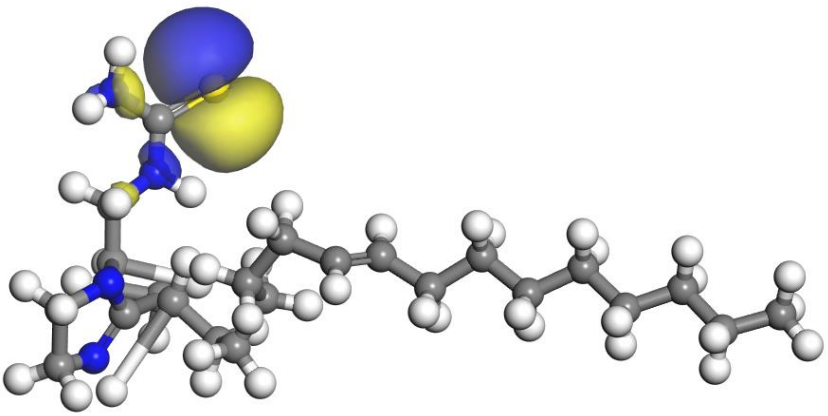

TAI-HOMO

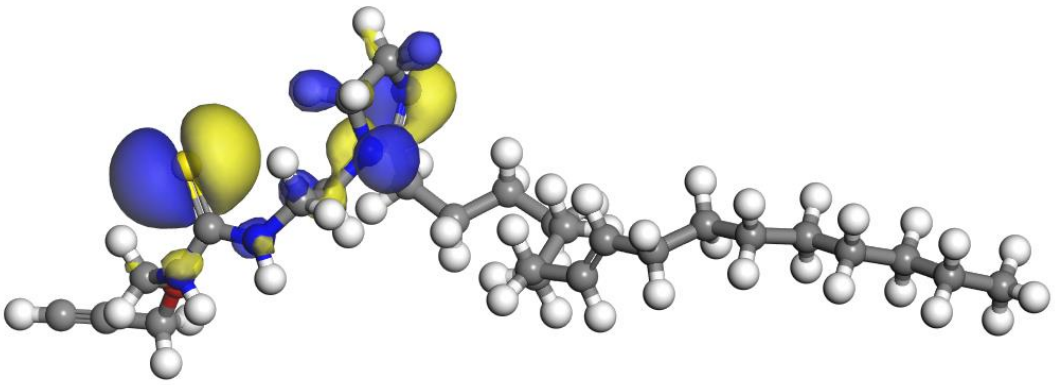

MTAI-HOMO

Figure 11. HOMO distribution of TAI and MTAI

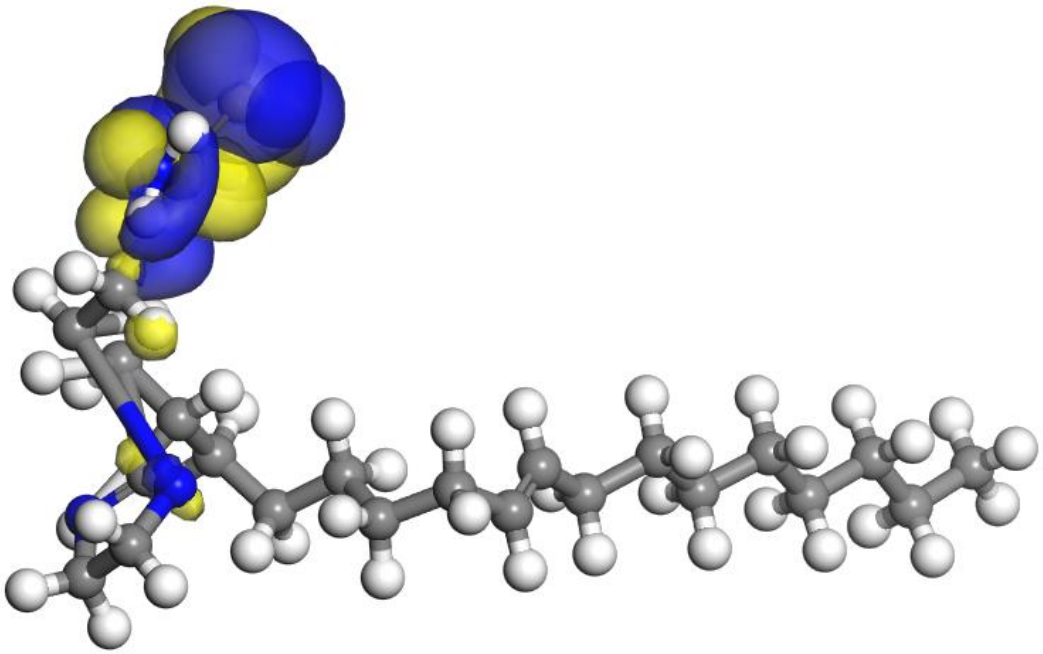

TAI-LUMO

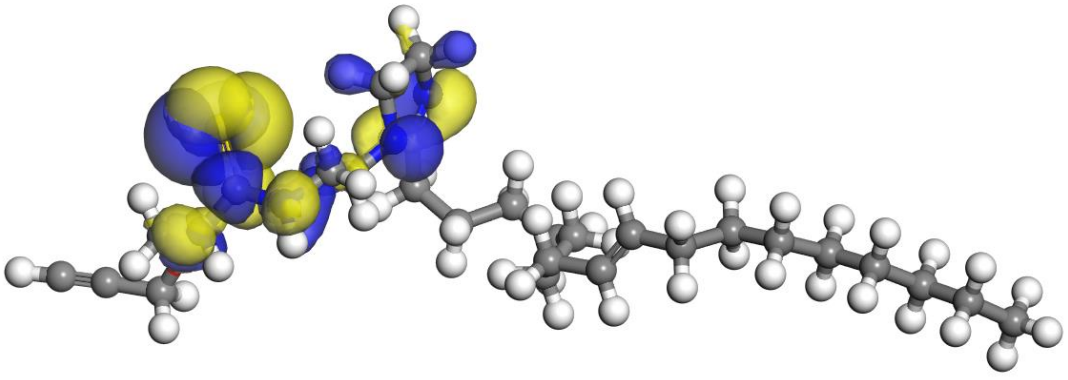

MTAI-LUMO

Figure 12. LUMO distribution of TAI and MTAI

Table 7. Orbital energies of TAI and MTAI

	E_{HOMO} (eV)	E_{LUMO} (eV)	ΔE (eV)
TAI	-5.114	0.287	5.401
MTAI	-5.576	-0.392	5.184

Table 8. Mulliken charges of non-hydrogen atoms

TAI	f^-	f^+	MTAI	f^-	f^+
C (1)	-0.001	-0.001	C (1)	-0.001	-0.001
C (2)	-0.001	-0.002	C (2)	-0.001	-0.001
C (3)	-0.001	-0.001	C (3)	-0.001	-0.001
C (4)	-0.001	-0.002	C (4)	-0.001	-0.001
C (5)	0	-0.001	C (5)	-0.001	0
C (6)	-0.002	-0.003	C (6)	-0.002	-0.001
C (7)	0	-0.003	C (7)	0	0
C (8)	-0.002	-0.006	C (8)	-0.004	-0.003
C (9)	0.006	0.017	C(9)	0.008	0.006
C (10)	-0.002	0.006	C (10)	-0.005	-0.005
C (11)	0.002	-0.003	C (11)	0.002	0.002
C (12)	-0.002	-0.005	C (12)	0	0.003
C (13)	0.005	-0.002	C (13)	-0.002	-0.002
C (14)	-0.005	-0.01	C (14)	-0.006	-0.004
C (15)	0.004	-0.013	C (15)	-0.006	0
C (16)	-0.01	-0.016	C (16)	-0.01	-0.002
C (17)	-0.007	0.065	C (17)	0.017	-0.005
N (18)	-0.006	0.051	N (18)	0.08	0.004
N (19)	-0.004	0.007	N (19)	0.097	0.03
C (20)	-0.004	-0.018	C (20)	-0.019	-0.008
C (21)	-0.004	-0.011	C (21)	-0.022	-0.007
C (49)	-0.002	-0.009	C (57)	-0.005	-0.004
C (52)	-0.013	-0.019	C (60)	-0.025	-0.005
C (53)	-0.04	-0.03	C (61)	-0.025	-0.027
N (54)	0.033	0.033	N (62)	0.019	0.051
C (68)	0.032	0.082	C (63)	0.026	0.152
S (69)	0.593	0.229	N (64)	0.015	0.033
N (70)	0.035	0.037	S (65)	0.294	0.312
			C (72)	-0.014	-0.005
			O (73)	-0.007	-0.013
			C (74)	-0.009	-0.009
			C (75)	-0.023	-0.025
			C (76)	0.031	0.055

4. CONCLUSIONS

(1) An imidazoline derivative containing sulfur and an alkynyl group has been successfully synthesized in this work.

(2) This imidazoline derivative shows high inhibition performance in a CO_2/H_2S system. The efficiency reaches 93.94% when used at only 20 ppm.

(3) The imidazoline obeys the Langmuir isotherm, and the adsorption of the inhibitor is of a chemical nature.

(4) The imidazoline derivative has two adsorption centres and a lower energy gap between LUMO and HOMO than that of thioureido-oleic acid imidazoline.

(5) The corrosion inhibition mechanism is mainly due to the adsorption of inhibitors on the steel surface, which protects the substrate from corrosion.

References

1. M.B. Kermani, A. Morshed, *Corrosion*, 59 (2003) 659.
2. G. Fierro, G.M. Ingo, F. Mancia, *Corrosion*, 45 (1989) 814.
3. K. Masamura, S. Hashizume, J. Sakai, I. Matsushima, *Corrosion*, 43 (1987) 359.
4. C. Zhang, J.M. Zhao, *Int.J.Electrochem.Sci.*, 12 (2017) 9161-9179.
5. P. Rajeev, A.O. Surendranathan, *J. Mater. Environ. Sci.*, 3 (2012) 856.
6. J.L.Crolet, *Applied Sciences*, 266 (1994) 1.
7. W. He, *Corros. Sci.*, 51 (2009) 2811.
8. G.A. Zhang, Y. Zeng, X.P. Guo, F. Jiang, D.Y. Shi, Z.Y. Chen, *Corros. Sci.*, 65 (2012) 37.
9. C. Zhang, J.M. Zhao, *Corros. Sci.*, 126 (2017) 247.
10. X. Li, X. Xie, J. *Taiwan Inst. Chem. Eng.*, 45 (2014) 3033.
11. P.M. Dasami, K. Parameswari, *Chitra S.*, 69 (2015) 195.
12. S.W. Xie, Z. Liu, G.C. Han, W. Li, J. Liu, Z. Chen, *Comput. Theor. Chem.*, 1063 (2015) 50.
13. M. Elachouri, M.S. Hajji, S. Kertit, E.M. Essassi, M. Salem, R. Coudert, *Corros. Sci.*, 37 (1995) 381.
14. B. Mernari, H. E. Attari, M. Traisnel, F. Bentiss, M. Lagrenee, *Corros. Sci.*, 40 (1998) 391.
15. G. Schmitt, *Br. Corros. J.*, 19 (1984) 165.
16. Y. Loidreau, E. Deau, P. Marchand, *Eur. J. Med. Chem.*, 92 (2015) 124.
17. J.M. Zhao, H.B. Duan, R.J. Jiang, *Corros. Sci.*, 91 (2015) 108.
18. F. Fei, J. Hu, J. Wei, Q. Yu, Z. Chen, *Constr. Build. Mater.*, 70 (2014) 43.
19. M. Yadav, D. Behera, U. Sharma, *Arab. J. Chem.*, 9 (2016) 1487.
20. Y. Zuo, Li. Y, Y. Tan, Y. Wang, J. Zhao, *Corros. Sci.*, 120 (2017) 99.
21. De.C. Waard, D.E. Milliams, *Corrosion*, 31 (1975) 177.
22. Y.J. Tan, S. Bailey, B. Kinsella, *Corros. Sci.*, 38 (1996) 1545.
23. V. Ramachandran, S. Jovancicevic, *Corrosion*, 55 (1999) 259.
24. W. Dumie, B. Kinsella, R.De. Marco, A. Jefferson, *J. Appl. Electrochem.*, 31 (2001) 1221.
25. A.M. Al-sabbagh. *Anti-corrosion Method M.*, 43 (1996) 11.
26. J.M. Zhao, G.H. Chen, *Electrochimica Acta*, 69 (2012) 247.
27. X. Jiang, Y. Zheng, W. Ke, *Corros. Sci.*, 47 (2005) 2636.
28. B. Wang, M. Du, J. Zhang, C.J. Gao, *Corros. Sci.*, 53 (2011) 353.
29. J.M. Zhao, F. Gu, T. Zhao, R.J. Jiang, *Res Chem Intermed.*, 42 (2016) 5753.
30. L.M. Rodriguez-Valdez, W. Villamisar, M. Casales, J.G. Gonzalez-Rodriguez, A. Martinez-Villafane, L. Maritinez, D. Glossman-Mitnik, *Corros. Sci.*, 48 (2006) 4053.

31. K.G. Zhang, Xu. B, W.Z. Yan, X.S. Yin, Y. Liu, Y. Chen, *Corros. Sci.*, 90 (2015) 284.
32. L.M. Rivera-Grau, M. Casales, I. Regla, D.M. Ortega-Toledo, D. Cuervo, J. Asencio, J.G. Gonzalez-Rodriguez, *Int. J. Electrochem. Sci.*, 7 (2012) 12610.
33. S.Q. Hu, J.C. Hu, C.C. Fan, S.Q. Mi, J. Zhang, W.Y. Guo, *Acta Phys. -Chim. Sin.*, 26 (2010) 2163.
34. Y. Fu, A. Manthiram, M.D. Guiver, *Electrochem. Commun.*, 8 (2006) 1386.
35. Y. Zuo, L. Yang, Y.J. Tan, Y.S. Wang, J.M. Zhao, *Corros. Sci.*, 120 (2017) 99.
36. R.C. Nascimento, L.B. Furtado, O.C. Guimarães Maria José, *J. Mol. LIQ.*, 256 (2018) 548.
37. Z. Petrovic, M. Metikos-Hukovic, R. Babic, *Prog. Org. Coat.*, 61 (2008) 1.
38. G.M. Li, *Anti-corrosion Method M.*, 50 (2003) 410.
39. I. Sckine, Y. Hirakawa, *Corrosion*, 42 (1986) 272.
40. L.B. Tang, G.N.Mu, G.H. Liu, *Corros. Sci.*, 45 (2003) 2251.
41. X.H. Li, G.N. Mu, *Applied Surface Science*, 252 (2005) 1254.
42. J. Zhang, J.X. Liu, W.Z. Yu, Y.G. Yan, L. You, L.F. Liu, *Corros. Sci.*, 52 (2010) 2059.
43. M. Luz, A. Rodriguez-Valdez, D. Glossman-Mintnik, 716 (2005) 61.
44. S.K. Shukla, M.A. Quraishi, *Corros. Sci.*, 51 (2009) 1007.
45. R. Fuchs-Godec, V. Dolecek, *Colloid. Surfaces. A*, 244 (2004) 73.
46. J. Zhang, G.M. Qiao, S.Q. Hu, Y.G. Yan, Z.J. Ren, L.J. Yu, *Corros. Sci.*, 53 (2011) 147.
47. J.M. Costa, J.M. Lluch, *Corros. Sci.*, 24 (1984) 929.